

waveguide frequency doubling element, and a low-voltage phase modulation element into a single, monolithic, planar light-wave circuit (PLC). The PLC concept advances NASA's future lidar systems due to its compact, efficient and reliable design, thus enabling use on small aircraft and satellites. The immediate application for this technology is targeted for NASA Langley's HSRL system for aerosol and cloud characterization. This Phase I effort proposes the development of a potassium titanyl phosphate (KTP) waveguide phase modulator for future integration into a PLC.

For this innovation, the proposed device is the integration of a waveguide-based frequency doubler and phase modulator in a single, fiber pigtail device that will be capable of efficient second harmonic generation of 1,064-nm light and subsequent phase modulation of the 532-nm light at 250 MHz, providing a properly spectrally formatted beam for HSRL's seed laser locking system. Fabrication of the integrated PLC chip for NASA Langley, planned for the Phase II effort, will require full integration and optimization of the waveguide components (SHG waveguide, splitters,

and phase modulator) onto a single, monolithic device. The PLC will greatly reduce the size and weight, improve electrical-to-optical efficiency, and significantly reduce the cost of NASA Langley's current stabilized HSRL seed laser system built around a commercial off-the-shelf seed laser that is free-space coupled to a bulk doubler and bulk phase modulator.

This work was done by Anthony Cook of Langley Research Center and Shirley McNeil, Gregg Switzer, and Philip Battle of AdvR, Inc. Further information is contained in a TSP (see page 1). LAR-17568-1

On Calculating the Zero-Gravity Surface Figure of a Mirror

As well as gravity reversing between two configurations, mount forces must reverse to within the St. Venant scale.

NASA's Jet Propulsion Laboratory, Pasadena, California

An analysis of the classical method of calculating the zero-gravity surface figure of a mirror from surface-figure measurements in the presence of gravity has led to improved understanding of conditions under which the calculations are valid. In this method, one measures the surface figure in two or more gravity-reversed configurations, then calculates the zero-gravity surface figure as the average of the surface figures determined from these measurements. It is now understood that gravity reversal is not, by itself, sufficient to ensure validity of the calculations: It is also necessary to reverse mounting forces, for which purpose one must ensure that mounting-fixture/mirror contacts are located either at the same places or else sufficiently close to the same places in both gravity-reversed configurations. It is usually not practical to locate the contacts at the same places, raising the question of how close is sufficiently close. The criterion for sufficient closeness is embodied in the St. Venant principle, which, in the present context, translates to a requirement that the distance between corresponding gravity-reversed mounting positions be small in comparison to their distances to the optical surface of the mirror.

The necessity of reversing mount forces is apparent in the behavior of the equations familiar from finite element analysis (FEA) that govern deformation of the mirror. In FEA, the three-dimensional solid body (mirror) is approximated by a mesh of N points, and positions of these points, or nodes, are

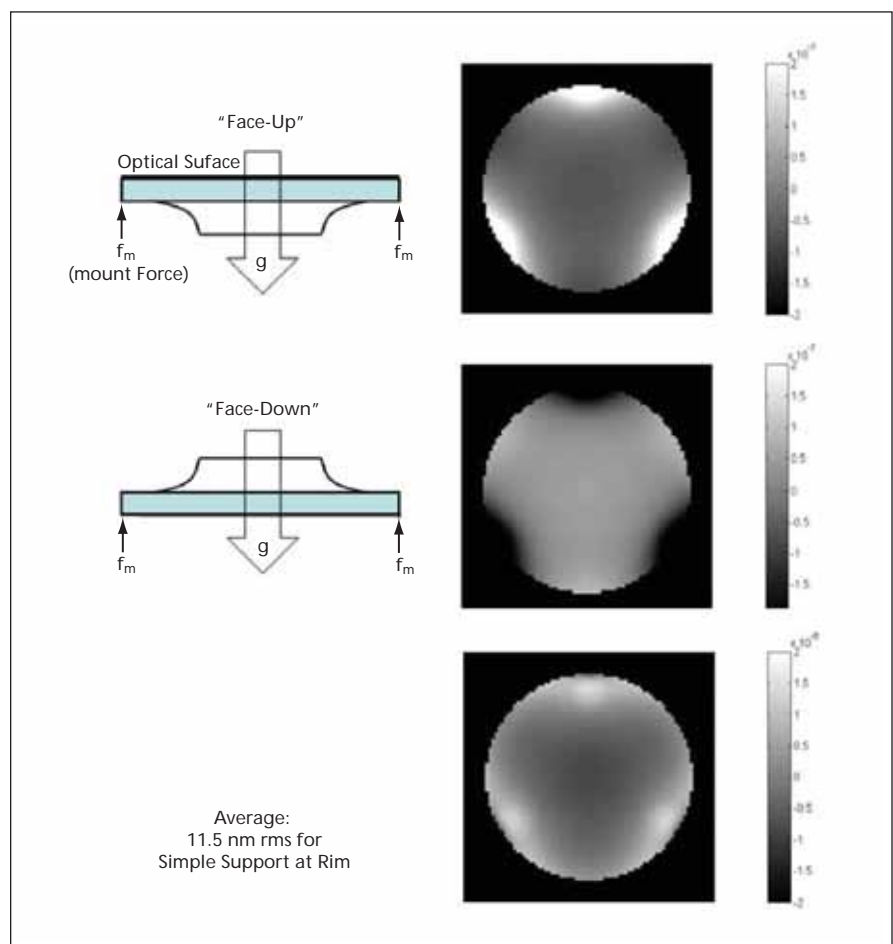


Fig. 1. FEA Modeling of the Surface Figure of PT-M1 during gravity reversal in a simple mirror mount in which the mirror rests on 3 points of contact near the rim (cartoons at left). The mirror model is specified to have a spherical surface in the absence of applied forces. The "face-up" and "face-down" orientations experience gravity forces that are reversed. However, mount forces in the two cases are applied at positions separated by the thickness of the mirror rim, so are only imperfectly reversed. Deformations in the two configurations are shown in the top two panels; their average is shown in the bottom panel, which recovers the ideal spherical surface (which would look flat in this display of departure from sphericity) marred by some dimple artifacts near the rim. The rms error in the average is 11.5 nm.

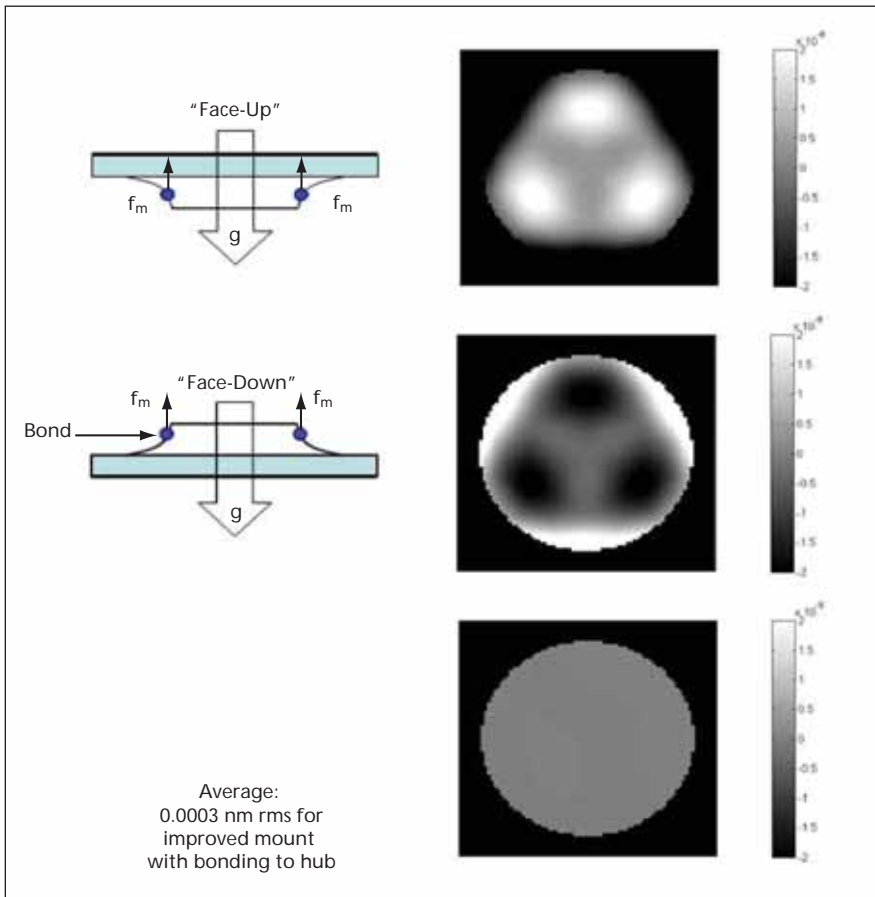


Fig. 2. FEA Modeling of the Surface Figure of PT-M1 during gravity reversal in an improved scheme incorporating good mount force reversal. The mount now consists of 3 point contacts bonded to the hub at the back of the mirror (cartoons at left); mount forces thus reverse and are applied at very nearly the same positions in the two orientations, far from the mirror surface. As a result, the surface figures (top two panels at right) are nearly exactly complementary, resulting in an average map (lower right panel) with a formal rms error of only 0.0003 nm.

represented by a $3N$ -dimensional coordinate vector \mathbf{x}_i . In the absence of forces, node positions are described by the zero-gravity position vector \mathbf{x}_i^{0g} that we wish to extract. Forces, also represented by a $3N$ -dimensional vector \mathbf{f}_i , cause deviations $\delta\mathbf{x}_i$ from the zero-gravity mirror shape; the case of interest is normal gravity ($1g$), for which we may write the altered elemental positions as

$$\mathbf{x}_i^{1g} = \mathbf{x}_i^{0g} + \delta\mathbf{x}_i \quad (1)$$

These forces may be either body forces due to gravity (\mathbf{f}^g) or boundary forces due to the mirror mount (\mathbf{f}^m). The displacements may then be found from

$$A_{ij}\delta\mathbf{x}_j = \mathbf{f}_i = \mathbf{f}_i^g + \mathbf{f}_i^m \quad (2)$$

where paired indices are summed over in the usual convention, and A_{ij} is the “stiffness matrix”. The stiffness matrix is generally sparse, so that a given node is significantly affected only by a small number of nearby nodes; with suitable numbering, it will be nearly diagonal. In the mirror frame, the stiffness matrix does not change when the mirror is ro-

tated among orientations. If the mirror is rotated into a new orientation in which body forces due to gravity reverse direction, and assuming that mount forces reverse as well, the new set of surface displacements $\delta\mathbf{x}'_i$ will obey

$$A_{ij}\delta\mathbf{x}'_j = \mathbf{f}'_i = -\mathbf{f}_i^g - \mathbf{f}_i^m \quad (3)$$

in the frame of the mirror. Comparing to Equation (2) shows that

$$\delta\mathbf{x}'_j = -\delta\mathbf{x}_j \text{ for all } j \quad (4)$$

In other words, the average of the deviations from the ideal zero-gravity surface in the two orientations is zero, so the average figure is just the zero-gravity surface. Algebraically, this property may be expressed as

$$1/2(\mathbf{x}_i^{1g} + \mathbf{x}_i^{0g} + \delta\mathbf{x}_i + \mathbf{x}_i^{0g} + \delta\mathbf{x}'_i) = \mathbf{x}_i^{0g} \quad (5)$$

If forces do not reverse perfectly, localized surface artifacts or “dimples” will be seen on the zero-gravity mirror map. Precise gravity reversal is relatively easy to achieve, but some care must be taken to ensure that mount forces, \mathbf{f}_i^m , also reverse. Furthermore, the reversed mount forces must be applied at the

same points i of the mirror. The tolerance on placing mount forces in the two configurations is set by the St. Venant principle, which captures the basic annealing or space-averaging property of the elliptic partial differential equations governing solid-body deformations in the usual elastic, small-deformation regime. Remarkably, in practice, small position errors in force location are insignificant at distances through the glass of perhaps only 1.5 times their value.

A simple illustration of these principles is provided by the problem of mounting the PT-M1 mirror for zero-gravity surface figure testing. This mirror is a spherical prototype of the largest mirror of the SIM compressor in its former TMA (three-mirror anastigmat) design. The PT-M1 mirror measures about 343 mm in diameter, has a radius of curvature of about 2.2 m, and a surface quality spec of 6.3 nm rms ($\lambda/100$) under zero-gravity conditions. It has an areal density of 41.9 km-m⁻². This demanding surface spec, coupled with aggressive lightweighting, makes precise attention to mounting schemes critical during measurement of the zero-gravity surface if simple artifacts are to be avoided. A rudimentary mounting scheme for “face-up/face-down” measurements whose average will yield the zero-gravity surface is shown in Figure 1. Support against gravity is provided from beneath the rim of the mirror, at two slightly different positions in the two configurations, and the result in the averaged surface map is dimpling at the position of the mounting points. The attendant measurement error (11.5 nm rms) exceeds the mirror spec.

A simple improvement to the mounting scheme is shown in Figure 2. Mount members are now attached by bonding, so mount forces in the two configurations are applied at identical positions. Also, mount members are attached to the hub of the mirror, well away from the mirror surface whose zero-gravity figure is being measured; by the St. Venant principle, small errors in effective positioning of mount members have little effect when propagated to the mirror surface. The resulting error in the zero-gravity averaged map is now only 0.0003 nm rms.

The principles described here represent an explicit clarification and deeper understanding of a classical technique for extracting the zero-gravity surface figure of a mirror from measurements of

multiple mounting configurations in normal gravity. While FEA computations are used to analyze particular candidate sets of mount configurations, these principles allow model-free insight into new configurations that are likely to be use-

ful. Additional information and extensions of the particular mounting schemes presented here, including one that offers dramatically improved zero-gravity map fidelity without the need for bonding, are discussed in Bloemhof,

Lam, Fera, and Chang, *Appl. Opt.* Vol. 46, No. 31, p. 7670 (2007).

This work was done by Eric E. Bloemhof of Caltech for NASA's Jet Propulsion Laboratory. For more information, contact iaofice@jpl.nasa.gov.NPO-45685

Optical Modification of Casimir Forces for Improved Function of Micro- and Nano-Scale Devices

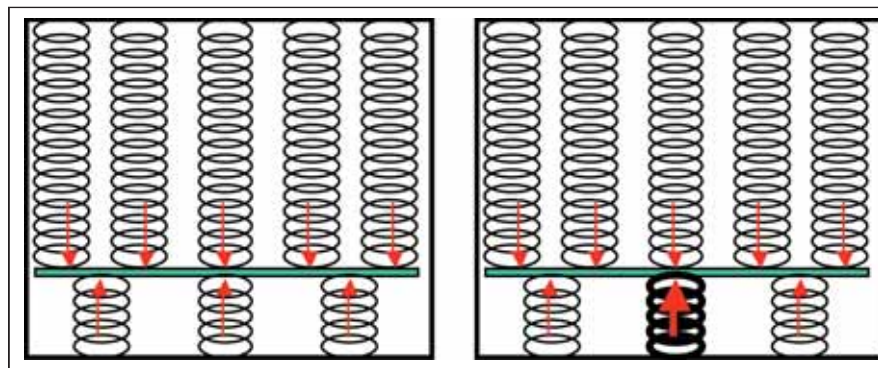
Manipulating these forces could result in improved MEMS devices.

NASA's Jet Propulsion Laboratory, Pasadena, CA

Recently, there has been a considerable effort to study the Casimir and van der Waals forces, enabled by the improved ability to measure small forces near surfaces. Because of the continuously growing role of micro- and nano-mechanical devices, the focus of this activity has shifted towards the ability to control these forces. Possible approaches to manipulating the Casimir force include development of composite materials, engineered nanostructures, mixed-phase materials, or active elements. So far, practical success has been limited. The role of geometrical factors in the Casimir force is significant. It is known, for example, that the Casimir force between two spherical shells enclosed one into the other is repulsive instead of normal attractive. Unfortunately, nanosurfaces with this topology are very difficult to make.

A more direct approach to manipulating and neutralizing the Casimir force is using external mechanical or electromagnetic forces. Unfortunately, the technological overhead of such an approach is quite large. Using electromagnetic compensation instead of mechanical will considerably reduce this overhead and at the same time provide the degree of control over the Casimir force that mechanical springs cannot provide. A mechanical analog behind Casimir forces is shown in the figure.

WGM (whispering gallery mode) resonators play an important role in modem optics and photonics because of their high quality factor and strong field localization. The optical field in such



A Mechanical Analog of the Casimir Force: On the left, a net force arises from the difference in the number of compressed springs (the optical modes) attached to two sides of a partition. On the right, the Casimir force can be compensated, or even reversed, by making a certain spring "tougher" (i.e., eternally pumping the optical mode).

resonators is localized near the surface, resulting in a strong evanescent field. A new method takes advantage of the evanescent field of optical WGMs and utilizes them to control the Casimir force at a metal-dielectric interface. The main novelty of the approach lies in combination of state-of-the-art techniques for measuring the Casimir force with the optical WGM microresonators. The WGM resonators shaped as microspheres will be used. The evanescent field emerging from the microresonator surface will enable the desired capability of manipulating, neutralizing, and reversing the Casimir force.

In real MEMS (microelectromechanical system) applications, it may or may not be possible to utilize the optical evanescent field technique. The proposed approach relies on modification of the electromagnetic energy density in a vacuum gap, rather than on modi-

fication of material properties or of the microdevice shape. The advantage of this approach is that the new knowledge and techniques developed in its framework will be applicable to a much broader class of MEMS affected by Casimir force, in particular to those of practical importance. The optical evanescent field is just one example of various surface excitations that can modify the energy density in small gaps, therefore changing the Casimir forces. As another example, forces can be mediated by exciting surface plasmons instead of the evanescent field photons. Therefore, it will be possible to directly apply these theoretical results and experimental techniques to realistic metallic or silicon MEMS.

This work was done by Dmitry V. Strelakov and Nan Yu of Caltech for NASA's Jet Propulsion Laboratory. Further information is contained in a TSP (see page 1). NPO-46672